

A Journal of the Gesellschaft Deutscher Chemiker

Angewandte Chemie

GDCh

International Edition

www.angewandte.org

Accepted Article

Title: Suprasomes Based on Host–Guest Molecular Recognition: An Excellent Alternative to Liposome in Cancer Theranostics

Authors: Kai Yang, Bin Hua, Shaolong Qi, Bing Bai, Chunyang Yu, Feihe Huang, and Guocan Yu

This manuscript has been accepted after peer review and appears as an Accepted Article online prior to editing, proofing, and formal publication of the final Version of Record (VoR). The VoR will be published online in Early View as soon as possible and may be different to this Accepted Article as a result of editing. Readers should obtain the VoR from the journal website shown below when it is published to ensure accuracy of information. The authors are responsible for the content of this Accepted Article.

To be cited as: *Angew. Chem. Int. Ed.* **2022**, e202213572

Link to VoR: <https://doi.org/10.1002/anie.202213572>

Suprasomes Based on Host–Guest Molecular Recognition: An Excellent Alternative to Liposomes in Cancer Theranostics

Kai Yang,^[a,b] Bin Hua,^[b] Shaolong Qi,^[a] Bing Bai,^[a] Chunyang Yu,^{*[c]} Feihe Huang,^[b] and Guocan Yu^{*[a]}

[a] K. Yang, Dr. S. Qi, Dr. B. Bai, Prof. Dr. G. Yu
Key Laboratory of Bioorganic Phosphorus Chemistry & Chemical Biology
Department of Chemistry, Tsinghua University
Beijing 100084, P. R. China
E-mail: guocanyu@mail.tsinghua.edu.cn

[b] K. Yang, Dr. B. Hua, Prof. Dr. F. Huang
Stoddart Institute of Molecular Science, Department of Chemistry, Zhejiang University, Hangzhou 310027, P. R. China
ZJU-Hangzhou Global Scientific and Technological Innovation Center, Hangzhou, 311215, P. R. China
Green Catalysis Center and College of Chemistry, Zhengzhou University, Zhengzhou 450001, P. R. China

[c] Prof. Dr. C. Yu
School of Chemistry and Chemical Engineering, State Key Laboratory of Metal Matrix Composites, Shanghai Jiao Tong University, 800 Dongchuan Road, Shanghai 200240, China
E-mail: chunyangyu@sjtu.edu.cn

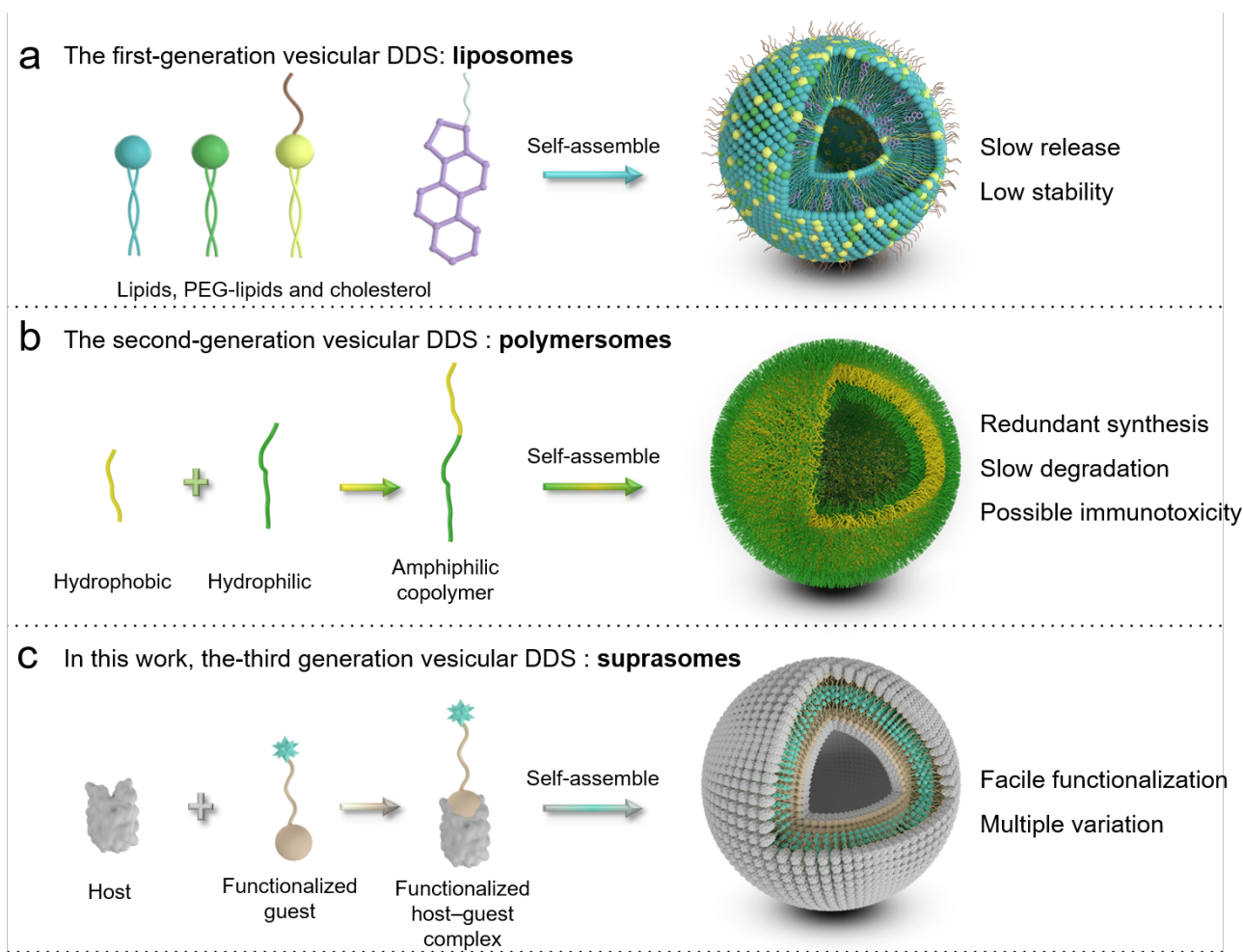
Abstract: Liposomes and polymersomes, typical vesicular drug delivery systems (DDSs), have faced some limitations in cancer theranostics. Suprasomes, supramolecular vesicles assembled from amphiphiles linked by noncovalent interactions, show potential as new generation of vesicular DDSs. We construct suprasomes based on host–guest recognition, by which the desired functions can be integrated into carriers without tedious synthesis. Photothermally active host–guest complex is formed between a functional guest and pillar[5]arene, which further self-assembles into hollow suprasomes. A supramolecular nanomedicine is developed by encapsulating cisplatin in the suprasomes. The obtained cisplatin@Suprasomes achieve excellent anticancer efficacy and anti-metastasis combining chemotherapy and photothermal therapy, which ablate the tumors without relapse and metastasis. This work demonstrates the facile functionalization of suprasomes, holding promise as alternatives to liposomes and polymersomes.

Introduction

Vesicles with hollow cavities are extensively used for delivering drugs in modern medicine, dramatically promoting specific biodistributions, enhancing therapeutic performances, and reducing side effects.^[1–5] As the first-generation vesicular drug delivery systems (DDSs), liposomes are self-assembled from lipids, polyethylene glycol (PEG)-lipids, and cholesterol in an aqueous solution (Scheme 1a).^[6–12] A variety of liposome-based drug formulations such as Onivyde (liposomal irinotecan) and Doxil (liposomal doxorubicin), have been approved by the Food and Drug Administration, and achieved prominent therapeutic performances. However, these natural materials are devoid of functionalization and stability, thus failing to meet the multiple requirements in clinic.^[13–14] As an alternative, the second-

generation vesicular DDSs, polymersomes prepared from amphiphilic copolymers have exhibited superior stability and abundant functionalizations compared to liposomes.^[15–19] Despite the merits that polymersomes possess, there still exist several obstacles, such as redundant synthesis, poor biodegradation, and possible long-term immunotoxicity, hampering their clinical applications.^[20–24] Therefore, it is imperative to develop the third-generation vesicular DDSs which feature facile functionalization and multimodality theranostics.

Different from liposomes and polymersomes, suprasomes, the vesicles based on supramolecular self-assembly can be the third generation of vesicular DDSs by manipulating noncovalent interactions (Scheme 1c). Among various supramolecular interactions, including hydrophobic interactions, electrostatic interactions, van der Waals forces, hydrogen bonds, hydrophobic interactions, and so on, host–guest recognitions are ideally suitable for the construction of suprasomes, owing to the facile functionalization, strong interactions, and stimuli-responsiveness between host and guest molecules.^[25–30] Benefiting from the dynamic nature of noncovalent host–guest interactions, theranostic moieties can be readily installed on the host or guest molecules to endow the suprasomes with theranostic properties and amphiphilicity. The suprasomes greatly overcome the limitations that liposomes and polymersomes faced, including monotonous performance and complex preparation.^[31–32] Notably, suprasomes are able to fully degrade into small molecules that can be rapidly excreted from the body, thus greatly reducing the toxicity caused by the exogenous nanocarriers. Therefore, suprasomes are supposed to hold the potential to be an excellent alternative to liposomes and polymersomes with promising applications in precise drug delivery.



Scheme 1. Schematic illustrations of the three generations of vesicular DDSs: a) liposomes, b) polymersomes and c) suprasomes.

Herein, the first paradigm of suprasomes is obtained through the boron dipyrromethene (BODIPY)-bearing methylimidazolium (**BDMI**)/pillar[5]arene host-guest molecular recognition and the self-assembly of such functionalized complex (Scheme 2). As shown in Scheme 2, the membrane of Suprasomes consists of a BODIPY-containing host-guest complex while cisplatin (CDDP) is encapsulated inside the cavity to afford chemotherapy.^[33-34] The heat produced from BODIPY upon laser irradiation not only provides photothermal therapy (PTT),^[35-36] but also spurs the release of CDDP from suprasomes, thus generating a spatiotemporally controllable drug release. Attributing to the suitable size and high stability of CDDP@Suprasomes in physiological environment, this supramolecular nanomedicine highly accumulates in tumor site of 4T1 tumor-bearing mice through the enhanced permeability and retention (EPR) effect with negligible premature leakage of loaded drugs.^[37] *In vivo* experiments reveal that the synergistic anticancer effect of PTT and chemotherapy completely ablates the primary tumor without metastasis, implying the promising future of suprasomes in cancer theranostics

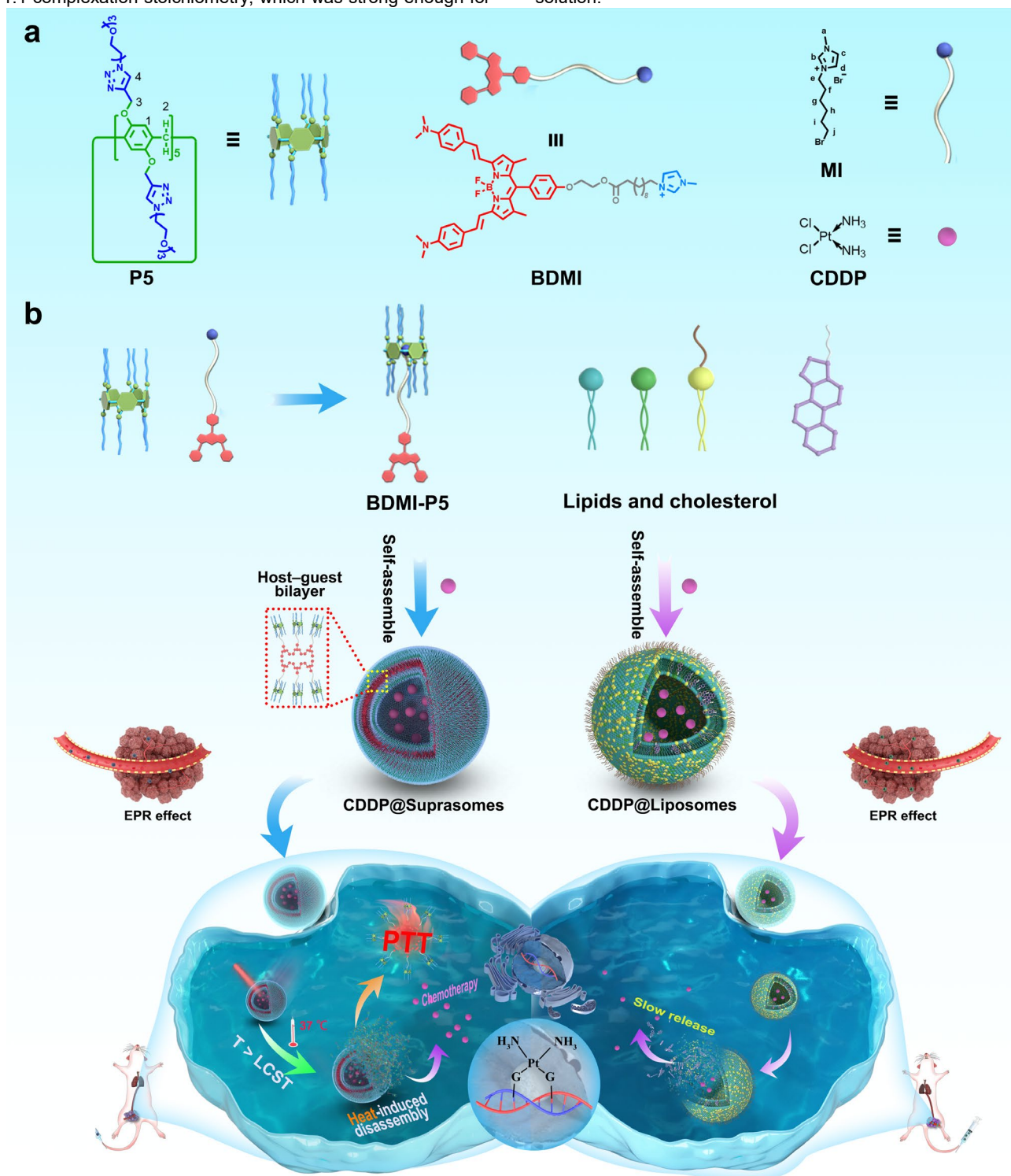
Results and Discussion

The fabricated suprasomes consisted of functionalized **BDMI** and pillar[5]arene modified by ten triethylene glycol monomethyl ether (**P5**), which were both easy to synthesize. **BDMI** was

mainly obtained through an esterification reaction to link BODIPY with alkyl chain-bearing methylimidazolium, and **P5** was obtained through a click reaction (Scheme S1 and Figure S1-7). Apart from the hydrophobic interactions between the alkyl chains, the BODIPY unit served as the photothermal reagent that could aggregate through π - π stacking, which significantly promoted the stability of suprasomes. We firstly utilized ^1H NMR spectroscopy to investigate the host-guest recognition using 1-hexyl-3-methylimidazolium bromide (**MI**) as a model guest compound. Compared with free **MI**, the splitting details of the signal related to protons on imidazole disappeared upon the addition of **P5** owing to the broaden effects (Figure 1b). Especially, the chemical shift of H^h was found below zero, confirming that the alkyl chain was positioned in the electron-sufficient cavity of **P5**. Besides, the formation of an inclusion complex between **P5** and **MI** resulted in modest chemical shift changes in resonance signals of **P5**. To better analyze the relative positions of the host-guest complex, a 2D NOESY NMR spectrum was performed. As shown in Figure 1d, significant NOE correlations between the signals of alkyl protons on **MI** and aromatic protons on **P5** were found, indicating the deep insertion of **MI** into the cavity of **P5**, and this was consistent with the findings in ^1H NMR spectra. The associate constant (K_a) of the host-guest complex was determined by ITC, providing the binding affinity and thermodynamic behaviors (Figure S8). The association

constant value was calculated to be $(2.86 \pm 0.41) \times 10^4 \text{ M}^{-1}$ with a 1:1 complexation stoichiometry, which was strong enough for

the fabrication of host-guest self-assembly in an aqueous solution.



Scheme 2. a) Chemical structures and cartoon representations of **P5**, **BDMI**, **MI**, and **CDDP**. b) Schematic illustration of the preparation of **CDDP@Suprasomes** and **CDDP@Liposomes**, and their antitumor process inside tumor cells. The **CDDP@Suprasomes** possess **PTT** and laser-triggered spatiotemporally controllable drug release.

After confirming the feasibility of forming a strong host-guest complex, we next studied the self-assembly behaviors using **BDMI** and **P5** with different ratios. The ratios of **BDMI** to **P5** were 1:3, 1:1, and 3:1, termed **P1B3**, **P1B1**, and **P3B1**. Dynamic light scattering (DLS) and transmission electron

microscopy (TEM) were performed to study the size distribution and morphology of the obtained self-assemblies. As shown in Figure 2a–d and Figure S9, the obtained nanostructures were solid nanoparticulate aggregates and the average size increased accompanied by the increase of the **P5** proportion, even

reaching a micron level. The size distribution variation indicated that particle size could be regulated by simply adjusting the ratio of host and guest molecules due to the dynamic properties. Notably, it was difficult to realize such size regulation in polymersomes, which was achieved by extensive screening of polymers with different hydrophobicity, exerting tedious work and high costs. More importantly, we successfully obtained Suprasomes with a diameter of ~95 nm (Figure 2e, g), and the drug-loaded nanoformulation CDDP@Suprasomes exhibited similar morphology as well as diameter shown in Figure 2f and g. It was noteworthy that the small windows on particles in Figure 2f revealed the hollow cavity in Suprasomes. Moreover, membrane structures with a thickness of 5–7 nm were observed in Figure 2e and f, illustrating the existence of vesicle structure. The stability of Suprasomes was evaluated by DLS analysis. After incubation in PBS for 24h, no obvious change in the mean diameter of Suprasomes was observed, demonstrating the excellent stability in physiological conditions, which was attributed to the strong noncovalent interactions, such as π - π stacking, hydrophobic interactions, and host-guest complexation (Figure 2h). UV-Vis absorption was conducted to study the photophysical behavior of Suprasomes (Figure S10). The obtained deep green dispersion solution of assemblies exhibited a typical spectrum corresponding to BODIPY, which is photothermally active.

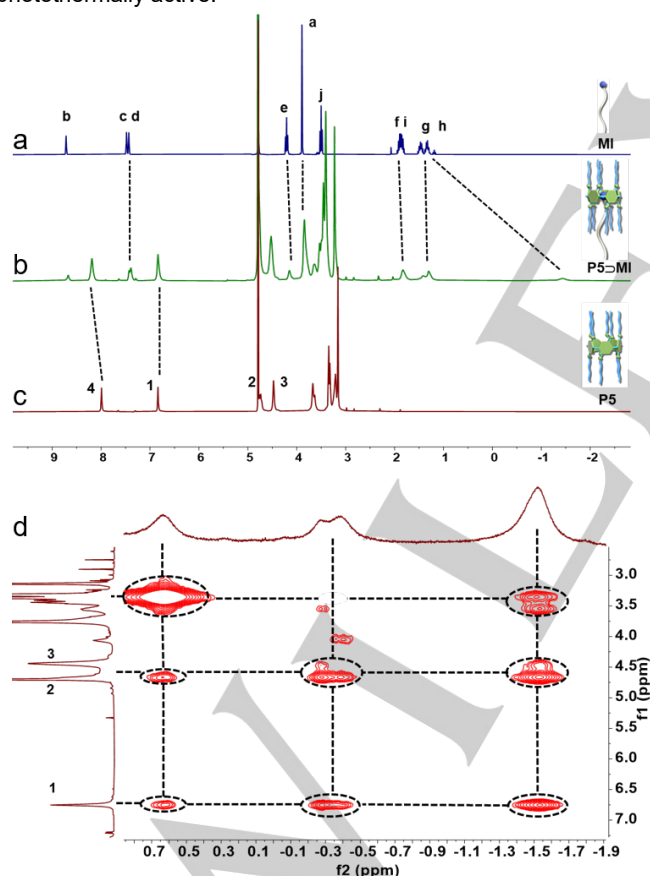


Figure 1. Partial ^1H NMR spectra of model host-guest interactions (400 MHz, D_2O , 295K): a) **MI** (2.00 mM); b) **MI** and **P5**; c) **P5**. d) 2D NOESY NMR spectrum (500 MHz, D_2O , 295 K) of **MI** and **P5**.

To disclose the interaction essence and the self-assembly dynamics, dissipative particle dynamics (DPD) simulations and quantum chemical computations were performed to reveal the

host-guest interactions and the self-assembly process of **BDMI-P5** and **P5** mixtures in solution (Scheme S2 and Table S1).^[38] Figure 2i–r represent the corresponding coarse-grain mapping, and snapshots of the self-assembly process of the **BDMI-P5** complex at various time intervals using DPD simulation. Beginning from a random stage (Figure 2i), the amphiphilic mixtures of the host-guest complex immediately aggregated into numerous small spherical micelles (Figure 2j). Afterward, these small micelles eventually fused to form a number of large spherical micelles (Figure 2k). Next, these large spherical micelles further fused with each other to form small disk-like micelles (Figure 2l), and eventually fused into one large curved membrane (Figure 2m–p). Thereafter, the membrane gradually bent and closed to form a regular spherical vesicle (Figure 3q–r). To further describe the vesicle microstructure, the density distribution from the mass center to its periphery was computed. The membrane structure of the vesicle is clearly depicted in Figure 2s, where the hydrophobic alkyl and aromatic segments (type A–D) distributed in the inner membrane of the Suprasomes, while the hydrophilic imidazole segment (type E) distributed in both the internal and external surfaces of the Suprasomes. In addition, it should be noted that the hydrophilic triethylene glycol segment (type F) is only distributed on the external surface of the Suprasomes due to the entropy effect. Then, we concluded the packing models of these molecules from simulation structures of Suprasomes. An illustration of the molecular packing model in a typical vesicle is given in Figure 2t. We found that there were two packing modes in the Suprasomes membrane and all of them presented as bilayer structures. The predicted vesicle membrane thickness was 6.80 nm, which was in good agreement with the experimental finding.

The photothermal effect of Suprasomes was evaluated in water. Upon laser irradiation (671 nm, 0.5 W cm^{-2}), the solution temperature of Suprasomes with the concentration of 0.50 mg/mL dramatically increased by about $33 \text{ }^\circ\text{C}$ within 150 s, while the temperature change of water was only $2 \text{ }^\circ\text{C}$, the sharp contrast highlighted the excellent photothermal conversion of Suprasomes (Figure 3a). In addition, the heat generated showed a concentration and time-dependent tendency upon laser irradiation, which meant the controllable photothermal effect. Notably, Suprasomes exhibited reliable photostability and thermal stability and negligible loss of photothermal performance was observed after 4 cycles of heating and cooling (Figure 3b). Moreover, the lower critical solution temperature (LCST) of Suprasomes was about $37 \text{ }^\circ\text{C}$, meaning that the photothermal effect-induced disassembly of Suprasomes could be precisely triggered upon laser irradiation, subsequently followed by the rapid release of loaded drugs (Figure 3c).^[39]

Considering the suitable LCST and excellent photothermal effect of Suprasomes, we evaluated the cumulative photothermal-triggered release of Suprasomes in an aqueous solution. Compared with the non-responsive CDDP@Liposomes, the content released from CDDP@Suprasomes reached 25.7% in 2 h after laser irradiation while CDDP@Liposomes released only 7.4% of loaded drugs at the same period (Figure 3d). Remarkably, 91.4% of loaded CDDP was released from CDDP@Suprasomes within 16 h after two exposures to laser irradiation, far beyond the cumulative release of 20.5% for CDDP@Liposomes, exhibiting extraordinary release efficiency under laser irradiation. In addition, Suprasomes alone released only 9.6% of encapsulated drugs within 24 h in the absence of

laser exposure, which demonstrated laser responsiveness and outstanding stability without stimuli. Besides, the morphology transformation of Suprasomes after the laser was monitored by TEM. As shown in Figure S11, the Suprasomes disassembled

after laser irradiation due to the heat generated from BODIPY, ensuring the rapid release of encapsulated drugs upon laser irradiation in tumor regions.

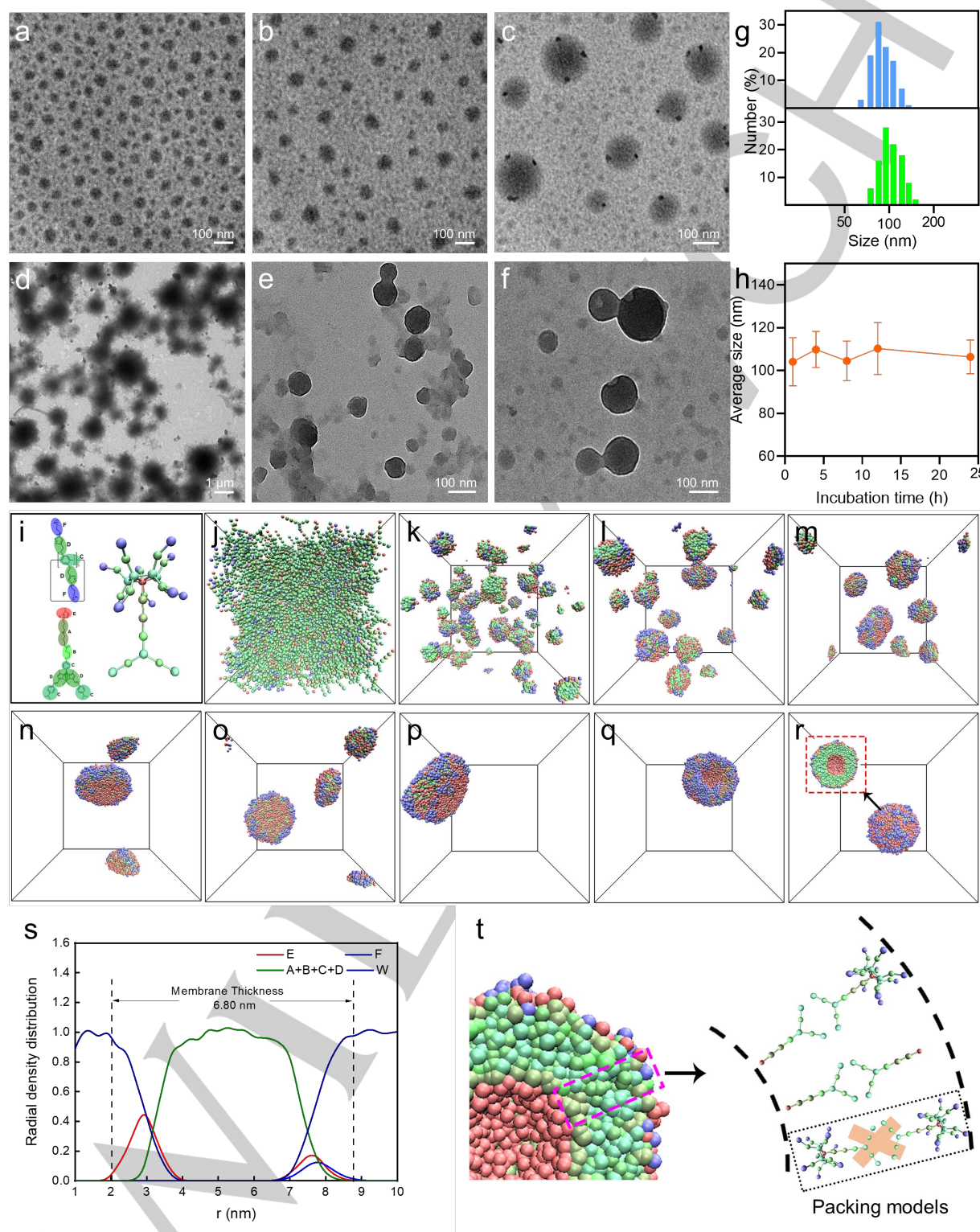


Figure 2. TEM images of a) P1B3, b) P1B1, c) P3B1, d) **BDMI**, e) Suprasomes and f) CDDP@Suprasomes. g) DLS size distribution of Suprasomes (blue) and CDDP@Suprasomes (green). h) Changes in the average diameter of Suprasomes in PBS over 24 h. i) The schematic model of molecule **BDMI**, **P5**, and **BDMI-P5** complex; j) Initial state. k) 5×10^4 time steps; l) 3×10^5 time steps; m) 8×10^5 time steps; n) 1.0×10^6 time steps; o) 1.5×10^6 time steps; p) 2.0×10^6 time steps; q) 2.6×10^6 time steps; r) 2.8×10^6 time steps. s) Radial density distributions of the different components in the vesicle. t) Illustration of the packing models of molecules within the vesicle membrane. The cross represents that such a packing model is not favorable. The solvent beads are removed for clarity.

Given that the endocytic pathways could affect uptake efficiency as well as the pharmacological activities of loaded drugs, we investigated the internalization pathways of Suprasomes by detecting the intracellular platinum amount through inductively coupled plasma mass spectrometry (ICP-MS) in the presence of endocytosis-associated inhibitors (Figure S12). The low cellular uptake efficiency at 4 °C suggested the energy-dependent endocytic pathways.^[40-41] Compared to amiloride (AMD) and genistein (Gen), 4T1 cells treated with

chlorpromazine (CPZ) exhibited relatively lower cellular internalization, which demonstrated that Suprasomes were mainly internalized by clathrin-mediated endocytosis. Therefore, the ingested Suprasomes would reside in the endosomes and macropinosomes, as evidenced by confocal laser scanning microscopy (CLSM), where well overlap between the red fluorescence arising from BODIPY units of Suprasomes and the green fluorescence of LysoTracker Green dye verified the distribution of Suprasomes in the cytoplasm (Figure 3e).

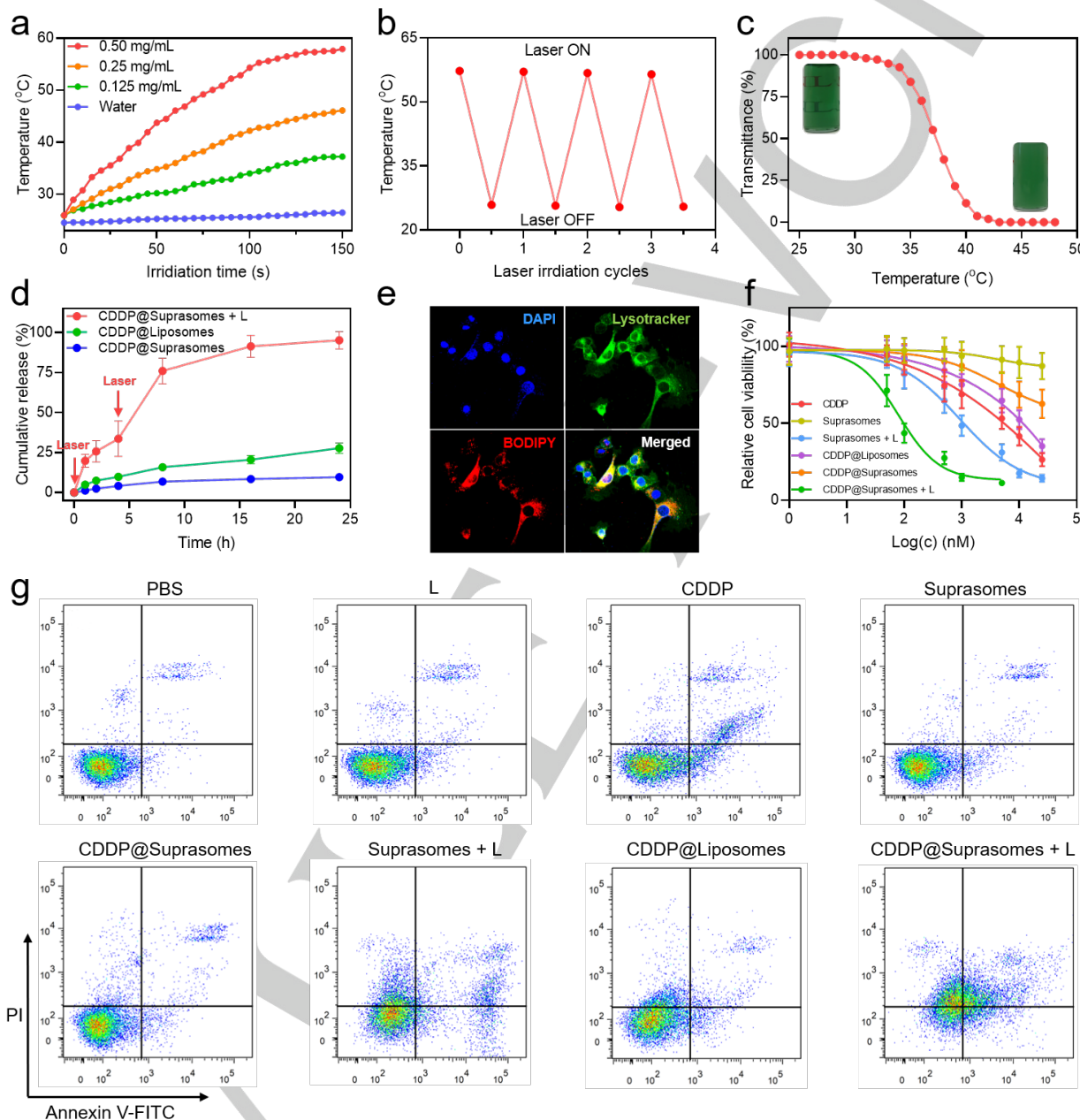


Figure 3. a) The concentration-dependent photothermal effect upon laser (671 nm, 0.5 W cm⁻²). b) Photostability results of Suprasomes after four cycles of irradiation. c) The transmittance curves of Suprasomes at a different temperature, the LCST was around 37 °C. d) Cumulative release curves of CDDP@Suprasomes + L, CDDP@Liposomes, and CDDP@Suprasomes alone. e) CLSM images of 4T1 cells cultured with Suprasomes towards 4T1 cells. f) Relative cell viability of 4T1 cells after different treatments g) Annexin V-FITC/PI staining of 4T1 cells after various treatments.

A 3-(4',5'-dimethylthiazol-2'-yl)-2,5-diphenyl tetrazolium bromide (MTT) assay was used to investigate the anticancer efficacies. Minimal variations in the relative cell activity were

observed for both host and guest molecules even at the concentration was up to 50.0 μM and 10.0 μM, respectively, demonstrating biocompatibility of the delivery vehicles (Figure

S13 and 14). The half-maximal inhibitory concentration (IC_{50}) of CDDP@Suprasomes + L is 84.9 ± 1.34 nM, which was significantly lower than those of Suprasomes + L (828 ± 52.1 nM) and CDDP (1520 ± 154 nM), revealing the extraordinary anticancer efficacies arising from the synergistic effect of chemotherapy and PTT (Figure 3f). Moreover, calcein acetoxymethyl ester and propidium iodide (PI) dual-staining were carried out to assess cell viability after various treatments (Figure S15, 16). Compared with chemotherapeutic groups including CDDP, CDDP@Liposomes, and CDDP@Suprasomes, significant anticancer efficacy was observed in PTT-treated groups, especially for CDDP@Suprasomes + L treatment which achieved complete cell apoptosis. In addition, flow cytometry using Annexin V-FITC and PI was utilized to further investigate the impact on cell viability induced by various treatments. As

shown in Figure 3g, a remarkable proportion of apoptosis/necrosis (69.0%) was detected in CDDP@Suprasomes + L treated groups, much higher than that of CDDP or Suprasomes + L treatments, implying the synergistic anticancer efficacy. Notably, compared to CDDP@Liposomes and CDDP@Suprasomes + L, the poor anticancer performance of PTT in anticancer therapy, but also confirmed the accelerated release of CDDP triggered by the photothermal effect-caused disruption of Suprasomes, which resulted in the highly effective concentration of CDDP to kill cancer cells. These data collectively demonstrated that CDDP@Suprasomes + L exhibited superb *in vitro* anticancer performance by the combination of PTT from vehicles and chemotherapy from rapid-released CDDP.

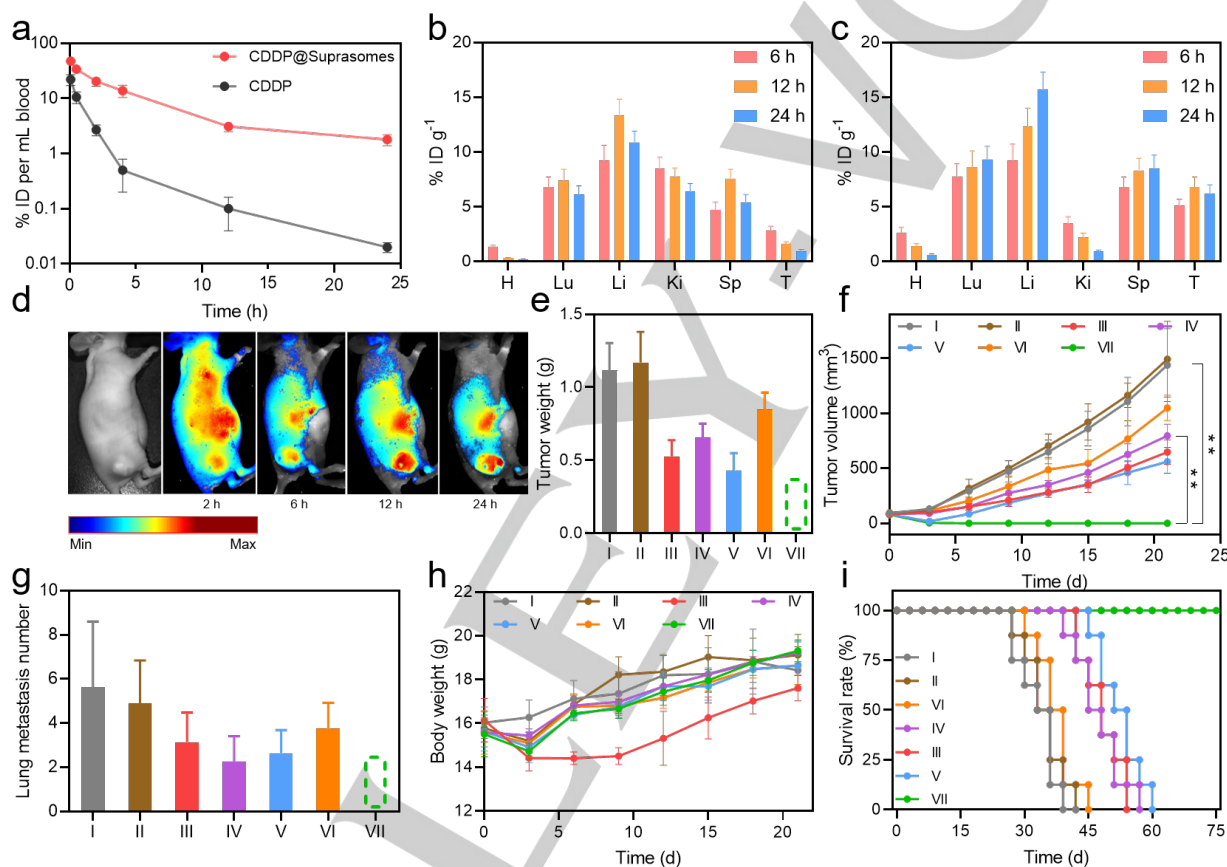


Figure 4. a) Blood circulation time of CDDP@Suprasomes and CDDP by measuring the concentration of Pt after i.v. injection. Tissue distribution of b) CDDP and c) CDDP@Suprasomes in main organs at different times after i.v. injection, H: heart, Lu: lung, Li: liver, Ki: kidney, Sp: spleen and T: tumor. d) FI of 4T1 tumor-bearing mice at different time post injection of Suprasomes. e) The average weight of tumors, and f) tumor growth inhibition curves after different treatments. ** $p < 0.01$. g) Lung metastasis number on lungs from mice after different treatments. h) Weight changes of mice bearing 4T1 tumors after various formulations. i) Kaplan–Meier survival rate. Groups: I, PBS; II, L; III, CDDP; IV, CDDP@Liposomes; V, Suprasomes + L; VI, CDDP@Suprasomes; VII, CDDP@Suprasomes + L.

Different from small molecular drugs suffering from short blood circulation time and rapid clearance, nanoformulation significantly prolonged retention time and promoted tumor accumulation benefiting from the EPR effect. Moreover, the triethylene glycol segments decorated on **P5** further prolong the retention time of Suprasomes by preventing clearance by the reticuloendothelial system. As shown in Figure 4a, after administration of CDDP@Suprasomes or CDDP for 12 h, 3.1% of the injected dose (ID) of CDDP@Suprasomes was detected

in the blood through ICP-MS, while CDDP remained only 0.1%. In addition, an intensive fluorescent signal was observed in the tumor area after administration of Suprasomes at 24 h post intravenous (i.v.) injection, demonstrating the enhanced tumor accumulation by virtue of EPR effects of nanocarriers (Figure 4d). Further evidence of enhanced tumor accumulation was obtained by quantitatively analyzing the biodistribution of Pt in tumor tissue and main organs (Figure 4b, c). Unexceptionally, small molecular CDDP showed relatively low Pt accumulation in

tumors with decreasing concentration over time, and relatively high accumulation in the lung, liver, kidney and spleen. Compared with free CDDP, nanoscale CDDP@Suprasomes exhibited significantly higher Pt concentration (about 6-fold) in tumor tissue and lower amount in the kidney after 24 h post-injection, revealing the enhanced accumulation in the tumor and potentially reduced cytotoxicity to kidney. It should be noted that a slightly higher concentration of Pt in the heart, lung, liver, and spleen was detected after treatment of CDDP@Suprasomes compared to CDDP, arising from the prolonged circulation time and the uptake by the reticuloendothelial system. Therefore, Suprasomes had successfully demonstrated excellent delivery capability as indicated by the high accumulation of Pt in tumor tissue, which guaranteed the chemotherapeutic efficiency.

To assess the comprehensive therapeutic performances of CDDP@Suprasomes featuring PTT and chemotherapy, the mice established orthotopic breast 4T1 tumors were administrated with different treatments, including phosphate buffer solution (PBS), laser (L), CDDP, CDDP@Liposomes, CDDP@Suprasomes, Suprasomes + L, and CDDP@Suprasomes + L. As shown in Figure 4f, the tumor volume of mice treated with PBS or laser increased quickly after 21 days, and the mean tumor volumes reached larger than 1300 mm³. Compared with the PBS-treated group, CDDP and CDDP@Liposomes showed moderate tumor inhibition with a mean tumor volume of 647 mm³ and 795 mm³, respectively. Suprasomes + L administration exhibited effective antitumor capability at the initial stage post-administration, however, failed to eliminate tumors adequately. Remarkably, among all treatments, significant antitumor efficacy was achieved by the CDDP@Suprasomes + L treatment with complete tumor clearance without relapse due to the synergistic effect of PTT and chemotherapy. The heat arising from BODIPY in suprasomes not only achieved PTT with outstanding antitumor performance but also triggered the disassembly of CDDP@Suprasomes followed by the rapid release of CDDP in tumors which led to the highly effective drug concentration, as evidenced by the unsatisfactory tumor inhibition of CDDP@Suprasomes and CDDP@Liposomes treatments. Tumor weight after treatments were assessed to further verify the effectiveness of CDDP@Suprasomes. In sharp comparison with other treatments exhibiting various tumor inhibition, no tumor was found in mice administrated with CDDP@Suprasomes + L, indicating unexceptionable antitumor performance (Figure 4e). Moreover, no lung metastasis was found in mice after treatment with CDDP@Suprasomes + L, suggesting remarkable anti-metastasis capability due to the superb anticancer efficacy for primary tumor and/or the micrometastasis inhibition from CDDP (Figure 4g, S17).

Typically, chemotherapy is accompanied by obvious side effects such as weight loss due to the systemic toxicity of drugs, impairing quality of life. We compared the impact of various therapeutic formulations on body weight, survival rate, and blood chemistry to evaluate their systemic toxicity. As shown in Figure 4h, mice treated with free CDDP suffered from serious weight fluctuations, demonstrating the strong side effects of CDDP. In sharp contrast, no weight fluctuations were observed in mice treated with CDDP@Suprasomes + L over the evaluation period, indicating the reduced systemic toxicity of CDDP encapsulated in Suprasomes. Moreover, Kaplan-Meier analyses revealed that compared to other therapeutic formulations with median survival

of no more than 54 days, no death was monitored in mice treated with CDDP@Suprasomes + L, confirming the superior antitumor efficacy and reduced side effects (Figure 4i). Furthermore, blood chemistry survey including alanine aminotransferase (ALT), alkaline phosphatase (ALP), aspartate aminotransferase (AST), blood urea nitrogen (BUN), and creatinine (CREA) showed that no observable differences were detected from mice treated with PBS, CDDP, and CDDP@Suprasomes, indicating that no hepatic or renal dysfunction occurred during the treatment (Figure S18). The hemolysis results demonstrated that Suprasomes did not cause hemolysis (Figure S19).

Since CDDP@Suprasomes + L has demonstrated great potential as novel a DDS, we further envision the possible forms of suprasomes. Suprasomes are functional vesicular DDS that multimodal theranostics can be simultaneously imported to generate a synergistic outcome. Benefitting from the facile synthesis of host-guest chemistry, various theranostic agents including chemotherapeutics, fluorescent imaging probes, metal-chelators, and targeting ligands can be easily integrated into the suprasomes to afford customized theranostics. Moreover, the dynamic nature and stimuli-responsiveness endow suprasomes with spatiotemporally controllable drug release, which can greatly improve drug efficacy and reduce side effects. In addition, various macrocyclic host molecules, such as pillararenes, cyclodextrins, and cucurbiturils are available building blocks for the construction of suprasomes, further satisfying the different requirements in disease treatment. Therefore, given the almost unlimited possible forms that suprasomes can adopt, suprasomes are highly promising to become the third generation of vesicular DDS.

Conclusion

In summary, we developed a novel therapeutic drug delivery platform named suprasomes based on host-guest molecular recognition between **P5** and **BDMI**, which will possibly be the third generation of vesicular DDSs. Benefitting from facile synthesis in supramolecular chemistry, excellent photothermal therapy was easily achieved by the introduction of BODIPY on carriers through host-guest interactions. Meanwhile, CDDP was encapsulated inside the cavity of Suprasomes to afford chemotherapy. Owing to the EPR effect, enhanced tumor accumulation of CDDP@Suprasomes was obtained, facilitating to promote the anticancer efficacy and reduce unwanted side effects. Moreover, the heat generated from BODIPY upon laser irradiation significantly accelerated the release of loaded CDDP, thereby realizing the highly effective drug concentration in tumor tissue, and eventually achieving superior anticancer performance by combining PTT and chemotherapy. Compared with PTT alone and traditional CDDP@Liposomes, *in vitro* and *in vivo* experiments demonstrated that treatment of CDDP@Suprasomes + L exhibited brilliant antitumor outcomes against orthotopic 4T1 breast cancer and anti-metastasis capability. Given the excellent synergistic effect of combined therapy and the complicated synthesis in the functionalization of traditional vectors, suprasomes possessing multiple theranostic functions have opened a prospective avenue for the functionalized carriers for precise drug delivery, emerging as excellent alternatives to liposomes and polymersomes.

Acknowledgements

F.H. thanks National Key Research and Development Program of China (2021YFA0910100) for financial support. G.Y. thanks the Vanke Special Fund for Public Health and Health Discipline Development, Tsinghua University (2022Z82WKJ005, 2022Z82WKJ013), the Tsinghua University Spring Breeze Fund (2021Z99CFZ007), the National Natural Science Foundation of China (22175107), a startup funding by Tsinghua University, and the Starry Night Science Fund of Zhejiang University Shanghai Institute for Advanced Study (SN-ZJU-SIAS-006) for financial support.

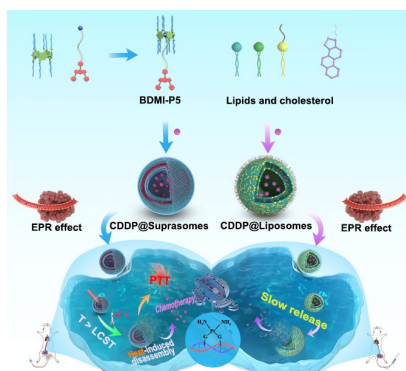
Competing financial interests

The authors declare no competing financial interests.

Keywords: cancer theranostics • drug delivery system • host-guest recognition • supramolecular chemistry • vesicles

- [1] M. A. Mintzer, E. E. Simanek, *Chem. Rev.* **2009**, *109*, 259-302.
- [2] B. S. Pattni, V. V. Chupin, V. P. Torchilin, *Chem. Rev.* **2015**, *115*, 10938-10966.
- [3] J. Zhou, L. Rao, G. Yu, T. R. Cook, X. Chen, F. Huang, *Chem. Soc. Rev.* **2021**, *50*, 2839-2891.
- [4] T. M. Allen, P. R. Cullis, *Adv. Drug. Deliv. Rev.* **2013**, *65*, 36-48.
- [5] D. A. LaVan, T. McGuire, R. Langer, *Nat. Biotechnol.* **2003**, *21*, 1184-1191.
- [6] D. J. Irvine, M. C. Hanson, K. Rakhra, T. Tokatlian, *Chem. Rev.* **2015**, *115*, 11109-11146.
- [7] N. Gong, N. C. Sheppard, M. M. Billingsley, C. H. June, M. J. Mitchell, *Nat. Nanotechnol.* **2021**, *16*, 25-36.
- [8] V. P. Torchilin, *Nat. Rev. Drug Discov.* **2005**, *4*, 145-160.
- [9] U. Sahin, P. Oehm, E. Derhovanessian, R. A. Jabulowsky, M. Vormehr, M. Gold, D. Maurus, D. Schwarck-Kokarakis, A. N. Kuhn, T. Omokoko, L. M. Kranz, M. Diken, S. Kreiter, H. Haas, S. Attig, R. Rae, K. Cuk, A. Kemmer-Bruck, A. Breitkreuz, C. Tolliver, J. Caspar, J. Quinkhardt, L. Hebich, M. Stein, A. Hohberger, I. Vogler, I. Liebig, S. Renken, J. Sikorski, M. Leierer, V. Muller, H. Mitzel-Rink, M. Miederer, C. Huber, S. Grabbe, J. Utikal, A. Pinter, R. Kaufmann, J. C. Hassel, C. Loquai, O. Tureci, *Nature* **2020**, *585*, 107-112.
- [10] Y. H. Choi, H. K. Han, *J. Pharm. Investig.* **2018**, *48*, 43-60.
- [11] Y. Barenholz, *J. Control. Release* **2012**, *160*, 117-134.
- [12] X. Zhou, S. Lin, H. Yan, *J. Nanobiotechnol.* **2022**, *20*, 257.
- [13] S. Mura, J. Nicolas, P. Couvreur, *Nat. Mater.* **2013**, *12*, 991-1003.
- [14] H. Chen, W. Zhang, G. Zhu, J. Xie, X. Chen, *Nat. Rev. Mater.* **2017**, *2*, 17024.
- [15] R. Duncan, *Nat. Rev. Cancer* **2006**, *6*, 688-701.
- [16] J. D. Robertson, G. Yealland, M. Avila-Olias, L. Chierico, O. Bandmann, S. A. Renshaw, G. Battaglia, *ACS Nano* **2014**, *8*, 4650-4661.
- [17] C. K. Wong, A. J. Laos, A. H. Soeriyadi, J. Wiedenmann, P. M. Curmi, J. J. Gooding, C. P. Marquis, M. H. Stenzel, P. Thordarson, *Angew. Chem. Int. Ed.* **2015**, *54*, 5317-5322. *Angew. Chem.* **2015**, *127*, 5317-5322.
- [18] D. Shae, K. W. Becker, P. Christov, D. S. Yun, A. K. R. Lytton-Jean, S. Sevimli, M. Ascano, M. Kelley, D. B. Johnson, J. M. Balko, J. T. Wilson, *Nat. Nanotechnol.* **2019**, *14*, 269-278.
- [19] H. Wang, S. Zhang, J. Lv, Y. Cheng, *View* **2021**, *2*, 20200026.
- [20] U. Kauscher, M. N. Holme, M. Bjornmalm, M. M. Stevens, *Adv. Drug Deliv. Rev.* **2019**, *138*, 259-275.
- [21] H. Sun, L. Mei, C. Song, X. Cui, P. Wang, *Biomaterials* **2006**, *27*, 1735-1740.
- [22] R. K. Jain, T. Stylianopoulos, *Nat. Rev. Clin. Oncol.* **2010**, *7*, 653-664.
- [23] N. Bertrand, J. Wu, X. Xu, N. Kamaly, O. C. Farokhzad, *Adv. Drug Deliv. Rev.* **2014**, *66*, 2-25.
- [24] S. Barua, S. Mitragotri, *Nano Today* **2014**, *9*, 223-243.
- [25] J. A. Hubbell, A. Chilkoti, *Science* **2012**, *337*, 303-305.
- [26] J. Zhou, G. Yu, F. Huang, *Chem. Soc. Rev.* **2017**, *46*, 7021-7053.
- [27] G. Yu, X. Zhao, J. Zhou, Z. Mao, X. Huang, Z. Wang, B. Hua, Y. Liu, F. Zhang, Z. He, O. Jacobson, C. Gao, W. Wang, C. Yu, X. Zhu, F. Huang, X. Chen, *J. Am. Chem. Soc.* **2018**, *140*, 8005-8019.
- [28] H. Wang, H. Wu, Y. Yi, K. F. Xue, J. F. Xu, H. Wang, Y. L. Zhao, X. Zhang, *CCS Chem.* **2021**, *3*, 1413-1425.
- [29] Y. C. Pan, X. Y. Hu, D. S. Guo, *Angew. Chem. Int. Ed.* **2021**, *60*, 2768-2794. *Angew. Chem.* **2021**, *133*, 2800-2828.
- [30] J. Ren, X. Shu, Y. Wang, D. Wang, G. Wu, X. Zhang, Q. Jin, J. Liu, Z. Wu, Z. Xu, C.-Z. Li, H. Li, *Chin. Chem. Lett.* **2022**, *33*, 1650-1658.
- [31] M. Elsbahy, K. L. Wooley, *Acc. Chem. Res.* **2015**, *48*, 1620-1630.
- [32] M. A. Dobrovolskaia, D. R. Germolec, J. L. Weaver, *Nat. Nanotechnol.* **2009**, *4*, 411-414.
- [33] D. Wang, S. J. Lippard, *Nat. Rev. Drug Discov.* **2005**, *4*, 307-320.
- [34] K. Mitra, S. Gautam, P. Kondaiah, A. R. Chakravarty, *Angew. Chem. Int. Ed.* **2015**, *54*, 13989-13993. *Angew. Chem.* **2015**, *127*, 14195-14199.
- [35] D. Xi, M. Xiao, J. Cao, L. Zhao, N. Xu, S. Long, J. Fan, K. Shao, W. Sun, X. Yan, X. Peng, *Adv. Mater.* **2020**, *32*, e1907855.
- [36] J. Mu, M. Xiao, Y. Shi, X. Geng, H. Li, Y. Yin, X. Chen, *Angew. Chem. Int. Ed.* **2022**, *61*, e202114722. *Angew. Chem.* **2022**, *134*, e202114722.
- [37] H. Maeda, J. Wu, T. Sawa, Y. Matsumura, K. Hori, *J. Control. Release* **2000**, *65*, 271-284.
- [38] Y. Liu, C. Yu, H. Jin, B. Jiang, X. Zhu, Y. Zhou, Z. Lu, D. Yan, *J. Am. Chem. Soc.* **2013**, *135*, 4765-4770.
- [39] T. Wolf, T. Rheinberger, J. Simon, F. R. Wurm, *J. Am. Chem. Soc.* **2017**, *139*, 11064-11072.
- [40] D. Yu, Y. Zhang, Z. Mao, C. Gao, *Macromol. Biosci.* **2013**, *13*, 1413-1421.
- [41] G. C. Yu, W. Yu, L. Shao, Z. H. Zhang, X. D. Chi, Z. W. Mao, C. Y. Gao, F. H. Huang, *Adv. Funct. Mater.* **2016**, *26*, 8999-9008.

Entry for the Table of Contents



Suprasomes, considered the third generation of vesicular drug delivery systems, are constructed based on host–guest recognition. Cisplatin-loaded suprasomes are promising for photothermal therapy (PTT) and laser-triggered spatiotemporally controllable drug release. Compared to liposomal nanomedicines, CDDP@Suprasomes realize complete tumor ablation without metastasis as a result of the synergy between PTT and chemotherapy, showing great potential in cancer theranostics.